Preprint-PSI-99-31
December 14, 1999

Higher Order Two Step Mechanisms in Nucleon Antinucleon Annihilation and the OZI Rule

S. von Rotz[a,b], M.P. Locher[a,b] and V.E. Markushin[a]

a) Paul Scherrer Institute, CH-5232 Villigen, Switzerland
b) University of Zurich, CH-8047 Zurich, Switzerland

Abstract

We evaluate three meson doorway mechanisms for nucleon-antinucleon annihilation at rest for the first time. Detailed results are presented for the final state $\phi\pi^0$ originating from the $^3S_1$ initial state and for the $\phi\rho$ channel originating from $^1S_0$. The results presented also include the improved contributions from two meson doorway states and from the tree diagrams. For all the channels considered a consistent explanation of large and small OZI violations emerges.

1 Introduction

Recent and accurate data for nucleon-antinucleon annihilation at rest from experiments performed at LEAR [1–8] have challenged our understanding of the underlying annihilation mechanisms and of the production of mesons with hidden strangeness in particular. Large violations of the OZI rule for special channels have been observed. The biggest deviation from the OZI prediction for hadronic channels occurs for the $\phi\pi^0$ final state and has led to speculations about the internal structure of the nucleon suggesting a large $s\bar{s}$ component in the wave function [9–11]. Earlier analysis [12–21] has shown that two meson doorway contributions have the correct magnitude to explain the experimental branching ratio for this reaction. The present paper extends the preceding calculations by including three meson doorway states. Sizable OZI-rule avoiding contributions are expected from such intermediate states since the first step, the annihilation into three non-strange mesons, represents about one third of the total annihilation cross section.

Based on the results of [22] we shall present a comprehensive effort of calculating all relevant diagrams involving (non-strange) three meson intermediate states leading to the two meson final states $\phi\pi^0$ and $\phi\rho^0$. The corresponding two-loop amplitudes have been evaluated with full spin. We have also completed the evaluation of one-loop amplitudes (two-meson-doorways) where needed. For completeness we report some of the results on other two-meson final states. We

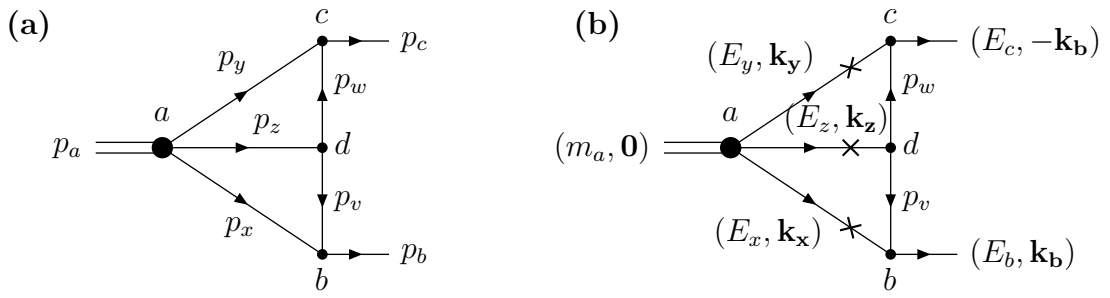

Figure 1: (a) The generic three-meson-doorway diagram; (b) unitarity approximation. The notation $p_n = (E_n, \mathbf{k_n})$ is used for the four–momenta of the particles $n = a, b, c, x, y, z, v, w$ in the CMS.

shall show that the results consistently explain the size of large and small OZI violations.

The paper is organized as follows. In Sec. 2 we describe the three meson doorway formalism. A generic case is reported in some detail while technicalities are relegated to the Appendices. Section 3 presents the three-meson-doorway results. Updated calculations for the two-meson doorway amplitudes are included and the full calculation is compared to the experimental branching ratios. Section 4 gives the conclusions.

2 Three-meson doorway mechanisms

The generic three-meson-doorway diagram is shown in Fig. 1 which also defines the notation in terms of four and three vectors. The crosses in Fig. 1(b) denote the unitarity approximation for which all the three s-channel particles are on their mass shell. The available data for the annihilation into three mesons relevant for the first step of the three-meson-doorway mechanisms are summarized in Table 7 of Appendix A.2.

The basic expression for the amplitude without spin is

$$T = \frac{i^2}{(2\pi)^8} \iint \frac{g_a g_b g_c g_d \, d^4p_x \, d^4p_y}{(p_x^2 - m_x^2 + i\epsilon)(p_y^2 - m_y^2 + i\epsilon)(p_z^2 - m_z^2 + i\epsilon)(p_v^2 - m_v^2 + i\epsilon)(p_w^2 - m_w^2 + i\epsilon)}. \tag{1}$$

where g_a, g_b, g_c, and g_d are the coupling constants corresponding to the vertices a, b, c, d in Fig. 1(a). In the on-shell or unitarity approximation Fig. 1(b), the amplitude T_{UA} has the form

$$T_{UA} \;=\; \frac{i g_a g_b g_c g_d}{2(2\pi)^5} \int \frac{d\Phi_3(p_a, p_x, p_y, p_z)}{(p_v^2 - m_v^2 + i\epsilon)(p_w^2 - m_w^2 + i\epsilon)} \tag{2}$$

where $d\Phi_3$ is the phase space of the intermediate three-meson state

$$d\Phi_3(p_a, p_x, p_y, p_z) \;=\; \delta(p_a - p_x - p_y - p_z) \frac{d^3\mathbf{k}_x}{2E_x} \frac{d^3\mathbf{k}_y}{2E_y} \frac{d^3\mathbf{k}_z}{2E_z} \tag{3}$$

The extension of Eqs.(1,2) to the case of particles with spin is straightforward. The details for the vertex spin structure and coupling constants used are given in Appendix A. The spin formalism for the overall amplitude of Fig.1 is summarized in Appendix B.

The leading two-loop mechanisms for the reactions $p\bar{p} \to \phi\pi^0$ correspond to the diagrams in Table 1. The $\phi\pi$ channel has $I^G = 1^+$ and originates from the $p\bar{p}(^3S_1)$ state $J^{PC} = 1^{--}$. Here we expect that the $\rho\pi\pi$ doorway mechanism is important because the $\rho\pi\pi$ system has the largest phase space among all three meson states with positive G-parity and is strongly produced in $p\bar{p}$ annihilation (see Appendix A, Table 7). The two-loop diagrams in Table 1 all proceed through the same doorway mesons ($\rho\pi\pi$) but differ by the mesons exchanged in the t-channel. The $\pi\pi$ subsystem in the intermediate state has total isospin $I = 0$ and total angular momentum $J = 0$. Thus there is no danger of double counting when this three-meson doorway mechanism is added to the two-meson $\rho\rho$ doorway mechanism which is known to be very important [19].

Spin effects have been calculated by introducing scalar invariant functions as described in Appendix B. As a cross check, helicity amplitudes for the full amplitude T have been evaluated, squared and summed. Several charge configurations for the intermediate states, see Table 1, add coherently leading to an enhancement of the two-loop contributions. The corresponding isospin factors are collected in Table 8 of Appendix B.1. Because the t-channel particles can reach the mass shell, the unitarity approximation acquires a real part. A similar situation has been encountered already in the one loop calculation for the two-meson doorway mechanism [19].

For the kinematical situations where the t-channel particles are off-shell we have introduced monopole form factors

$$F_b(\lambda_v) = \frac{\lambda_v^2 - m_v^2}{\lambda_v^2 - p_v^2} = \frac{\lambda_v^2 - m_v^2}{\lambda_v^2 - (p_b - p_x)^2} \tag{4}$$

$$F_c(\lambda_w) = \frac{\lambda_w^2 - m_w^2}{\lambda_w^2 - p_w^2} = \frac{\lambda_w^2 - m_w^2}{\lambda_w^2 - (p_b + p_y)^2}. \tag{5}$$

The parameters have been varied in the range $\lambda_v, \lambda_w = (1.0 - 1.5)$ GeV, similar to the one loop calculation [19]. The form factors reduce the unitarity amplitude by about a factor two. For a calculation beyond the unitarity approximation form factors for the s-channel doorway mesons must be introduced as well. The corresponding off–shell contributions are expected to be comparable to the unitarity amplitude, similar to the detailed evaluations done in the one-loop case [19].

Turning to the $\phi\rho$ channel which has $I^G = 1^-$ and originates from the $p\bar{p}(^1S_0)$ state $J^{PC} = 0^{-+}$, we expect that the $\pi\pi\pi$ and $\omega\pi\pi$ doorway mechanisms are important because these intermediate states have the largest phase space among all three meson states with negative G-parity. Several states for the $\pi\pi\pi$ system are possible in this case which can be classified by the symmetry of the isospin wave function. The completely symmetric isospin wave function corresponding

mechanism	$\lvert T/g^{\rm tree}_{a\to\phi\pi}\rvert$
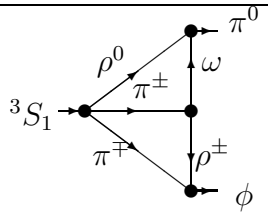	2.91
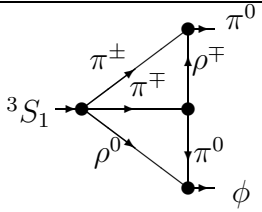	1.35
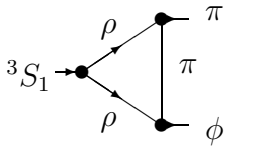	0.6 – 2.6
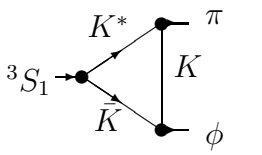	2.0 – 3.3
Experiment	7.0 $\pm$0.4 [7]

Table 1: Two-loop and one-loop diagrams for the reaction $p\bar{p}(^1S_0) \to \phi\pi$. The corresponding amplitudes T are normalized to the tree-level amplitude $g^{\rm tree}_{a\to\phi\pi}$ from $\omega\phi$ mixing.

mechanism	$\lvert T/g^{\rm tree}_{a\to\phi\rho}\rvert$
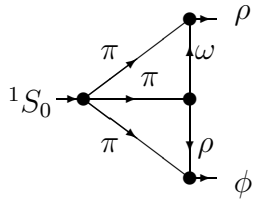	0.82
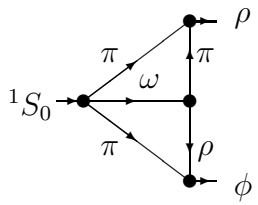	0.74
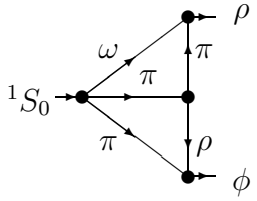	0.96
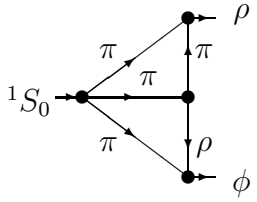	0.18
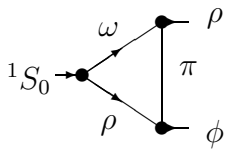	0.6
Experiment	4.9 $\pm$0.8 [2]

Table 2: Two-loop and one-loop diagrams for the reaction $p\bar{p}(^1S_0) \to \phi\rho$. The corresponding amplitudes T are normalized to the tree-level amplitude $g^{\rm tree}_{a\to\phi\rho}$ from $\omega\phi$ mixing.

to the Young tableau $\square\square\square$ has isospin $I = 1$ (another completely symmetric state $I = 3$ is excluded by isospin conservation) [23], with the space part being also completely symmetric. In Appendix A, the notation $g^A_{3\pi}$ is used for the corresponding coupling constant. The state with the mixed symmetry of the isospin part $\begin{array}{|c|c|}\hline \\ \hline\end{array}$ can also have total isospin $I = 1$, the corresponding coupling constant is $g^B_{3\pi}$ (see Appendix A for details). In this case the 3π state always contains a pion pair with total isospin $I_{\pi\pi} = 1$ and odd relative angular momentum. It is likely that this configuration is saturated by the $\rho^{\pm}\pi^{\mp}$ channel (the channel $\rho^0\pi^0$ is not coupled to the $\phi\rho^0$ because of wrong C-parity). We shall drop such three–meson intermediate states to avoid double counting. The completely antisymmetric isospin wave function has total isospin $I = 0$ and cannot occur in the annihilation into $\phi\pi$. Concerning the intermediate state $\omega\pi\pi$, its isospin structure is completely determined by the total isospin of the final state $I = 1$ which is equal to the isospin of the pion pair. Therefore one can expect that this intermediate state is saturated by the one-loop intermediate state $\omega\rho^0$. For the purpose of information the tables show all relevant amplitudes calculated separately. The two-loop contributions are fairly sizable.

3 Results

The complete results for the $\phi\pi^0$ and $\phi\rho^0$ channels are summarized in Tables 1, 2, and 3. The three-meson doorway states shown are the ones leading to the biggest contributions. The contributions from other intermediate states have been calculated and were found to be negligible [22]. The 'tree-level' amplitudes correspond to the $\omega\phi$ mixing which is proportional to the deviation of the physical mixing angle $\Theta = 37.6^o$ [24] from the the ideal one $\Theta_i = 35.3^o$:

$$g^{\rm tree}_{a\to\phi X} = \tan\left(\Theta - \Theta_i\right) \cdot g_{a\to\omega X} \quad . \tag{6}$$

The on-shell values of the vertex functions occurring in the calculation are constrained directly by experimental information. For the annihilation vertices, the data are shown in Table 7 and the corresponding coupling constants have been parametrized as described in Appendix A.2. The remaining vertices have been calculated from the measured decay widths of the corresponding mesons and are collected in Appendix A.1. The values shown in Table 3 do not include the form factors of Eqs.(4,5) which lead to a reduction by about a factor of two. This should be quite a reliable approximation since this reduction is expected to be partially compensated by contributions originating from off-shell s-channel propagation, similarly to the case of two-meson doorway mechanism [19], as mentioned in the context of Eqs.(4,5).

In general, major cancellations between amplitudes corresponding to different intermediate states are not likely to occur for the unitarity approximation. Because the main contribution in this case comes from the absorptive part of loop diagrams, the situation is very different from the well known case of Lipkin cancellations [25] where, contrary to our situation, threshold effects are negligible and

Reaction / Mechanism	$BR \cdot 10^4$
$p\bar{p} \to \phi\pi^0$ (tree-level)	0.13
$p\bar{p} \to K^*\bar{K} \to \phi\pi^0$	$0.5 - 1.4$
$p\bar{p} \to \rho\rho \to \phi\pi^0$	$0.05 - 2.0$
$p\bar{p} \to \phi\pi^0$ (1-loop)	$0.9 - 5.1$
$p\bar{p} \to \rho^0\pi\pi \to \phi\pi^0$	0.22
$p\bar{p} \to \pi\rho^0\pi \to \phi\pi^0$	1.1
$p\bar{p} \to \phi\pi^0$ (1-loop and 2-loop)	$5.9 - 17$
$p\bar{p} \to \phi\pi^0$ (**experiment**)	6.5 ± 0.7 [7]
	7.6 ± 0.6 [8]
	4.0 ± 0.8 [2]
$p\bar{p} \to \phi\rho^0$ (tree-level)	0.14
$p\bar{p} \to \phi\rho^0$ (one-loop)	0.1
$p\bar{p} \to \omega\pi\pi \to \phi\rho^0$	0.08
$p\bar{p} \to \pi\pi\pi \to \phi\rho^0$	0.10
$p\bar{p} \to \phi\rho^0$ (1-loop and 2-loop)	~ 2
$p\bar{p} \to \phi\rho^0$ (**experiment**)	3.4 ± 1.0 [2]
$p\bar{p} \to \phi\eta$ (tree-level)	0.2
$p\bar{p} \to K^*\bar{K} \to \phi\eta$	1.0
$p\bar{p} \to \phi\eta$ (**experiment**)	0.78 ± 0.21 [5]

Table 3: The branching ratios BR calculated for various doorway mechanisms in comparison with the experimental data (in units 10^{-4}). The values marked 1-loop and 2-loop contributions correspond to different ways of adding the amplitudes coherently.

specific intermediate states interfere distructively. In the case of the $\phi\pi$ channel the situation has been discussed in detail [19] for the one-loop mechanism.

For the case of the $\rho\rho$ doorway contribution to $\phi\pi^0$ we have evaluated the full range of the possible coupling constants, see Appendix C, complementing the results in [22]. The corresponding range is indicated in Table 3.

For the OZI–violating final state $\phi\pi^0$ the calculated branching ratio in Table 3 is well within the experimental range. The three–meson doorway contributions are comparable with the two–meson ones. The range of theoretical predictions when adding the amplitudes coherently now easily includes the experimental branching ratios while the one-loop results alone are somewhat low. For the $\phi\eta$ channel, the two-meson-doorway mechanism with the $K^*\bar{K}$ intermediate state has been found to be comparable with the experimental data. The two-loop calculations for the $\phi\rho$ final states are also reported in Table 3. As has been mentioned at the end of Section 2, two of the diagrams involve double counting with one-loop mechanisms, which is not easily quantified. However, the two-loop contributions obviously improve the comparison with the experimental branching ratio.

At the end of this section we would like to mention that we have also evaluated two and three-meson doorway contributions for a number of two meson final states ($\pi\pi$, $\rho\pi$, $\rho\rho$ and $\rho\omega$) without hidden strangeness. It is gratifying to observe that all the doorway contributions calculated have turned out to be relatively small when compared to the experimental rates for the corresponding annihilation channels.

4 Conclusions

We have found that the observed OZI violating enhancement of ϕ meson production at rest can be naturally explained by two and three meson doorway contributions. In our analysis, there appears to be no need to introduce a large $s\bar{s}$ fraction into the nucleon wave function. The doorway calculations presented here are well constrained by experimental information. In the first step of the doorway mechanism the annihilation rates into non-strange mesons enter. For annihilation at rest these transition rates are well measured. This is particularly true for the largest observed OZI violation in $p\bar{p} \to \phi\pi^0$ where detailed information on the spin–isospin dependence of the amplitudes for the annihilation $p\bar{p} \to K^*\bar{K}$ exists. Similarly the meson decay vertices occuring in the second step of the one–loop doorway mechanism are directly constrained by the measured decay widths. The leading one–loop contribution is thus well determined. In the present paper we have shown that the dominant three–meson doorway mechanisms (two loops) for $p\bar{p} \to \phi\pi$ are of similar size as the one loop contributions. It is therefore established that the full calculation leaves ample space for accommodating any remaining descrepancy with the measured branching ratio. At the same time two and three-meson doorway contributions to all the other channels involving ϕ mesons in the final state are small but not negligible due to interference, which again is in agreement with measured branching ratios. Four-meson-doorway contributions and higher are expected to be negligible due to progressively vanishing probability to rearrange non-strange multi-meson intermediate states into two–meson final states. We therefore believe that the present multiple doorway analysis is qualitatively exhaustive for nucleon-antinucleon annihilation into ϕ mesons at rest. Extending these calculations towards higher energies seems desirable. However, the experimental information on the energy dependence of the production of the intermediate states is far less detailed and large uncertainties in the corresponding predictions appear to be unavoidable.

Acknowledgment

We are grateful to M. Sapozhnikov for stimulating discussions. This paper was suppoted in part by the Swiss National Science Foundation.

A Coupling constants

In this appendix, we collect the coupling constants for $\bar{p}p$ annihilation at rest into various two and three-meson annihilation channels and the required coupling constants for meson decays. For most cases, the couplings can be expressed in terms of partial decay widths which are known from experiment and provide a model-independent input to the calculations of the doorway mechanisms.

A.1 Vertices for two-particle decays

The amplitudes corresponding to the transitions $a \to b+c$ involving pseudoscalar fields ϕ and vector fields V^μ with minimal number of derivatives have the following form in momentum space

$$\langle \phi_b \phi_c | T | V_a \rangle = g_{V\phi\phi}\, \varepsilon_a \cdot (p_b - p_c) \quad \text{(A1)}$$

$$\langle V_b \phi_c | T | V_a \rangle = g_{VV\phi}\, \epsilon_{\mu\nu\alpha\beta}\, p_a^\mu \varepsilon_a^\nu p_b^\alpha \varepsilon_b^\beta \quad \text{(A2)}$$

$$\langle V_b V_c | T | V_a \rangle = g_V^{(1)}\, p_a \cdot \varepsilon_b\, \varepsilon_a \cdot \varepsilon_c + g_V^{(2)}\, p_a \cdot \varepsilon_c\, \varepsilon_a \cdot \varepsilon_b + g_V^{(3)}\, p_b \cdot \varepsilon_a\, \varepsilon_b \cdot \varepsilon_c \quad \text{(A3)}$$

where p_a, p_b, p_c are the corresponding four-momenta, ε_a, ε_b, ε_c are the polarization vectors and $\epsilon^{\mu\nu\alpha\beta}$ is the totally antisymmetric Levi-Cività tensor. The decay widths $\Gamma_{a\to b+c}$ are related to the corresponding coupling constants g_{abs} by

$$\Gamma_{a\to b+c} = \frac{g_{abc}^2 f(k_{bc}) k_{bc}}{8\pi m_a^2} \quad \text{(A4)}$$

$$k_{bc} = \frac{\sqrt{(m_a^2 - (m_b+m_c)^2)(m_a^2 - (m_b-m_c)^2)}}{2m_a} \quad \text{(A5)}$$

where k_{bc} is the CMS momentum of the particles b ans c, m_a, m_b, and m_c are the corresponding particle masses and $f(k_{bc})$ are the spin-weight functions defined in Table 4.

The following coupling constants for the meson decays were used in the present calculations: $g_{\rho\pi\pi} = 6.00$, $g_{\phi K\bar{K}} = 4.6$, $g_{K^*K\pi} = 5.54$, $g_{\phi\rho\pi} = 1.86$ GeV^{-1}. The numerical values of the coupling constants for the two-meson $p\bar{p}$ annihilation are summarized in Tab. 5 together with the corresponding experimental branching ratios. For the sake of convenience, the $p\bar{p}$ annihilation coupling constants are normalized to the partial widths of the ground state of the $p\bar{p}$ atom. These partial widths are related to the corresponding annihilation cross sections $\sigma_{p\bar{p}\to b+c}$ by

$$\Gamma_{p\bar{p}\to b+c} = (v\sigma_{p\bar{p}\to b+c})_{v\to 0} |\psi_{1S}(0)|^2 \quad \text{(A6)}$$

where v is the relative velocity and $|\psi_{1S}(0)|^2 = \frac{\alpha^3 m_p^3}{8\pi}$ is the probability density for the $1S$ atomic state at zero separation between p and $\bar{p}$. This gives the following relation between the coupling constants listed in Table 5 and the S-wave annihilation amplitudes $g_{p+\bar{p}\to b+c}$ at zero energy:

$$g_{a\to b+c}^2 = g_{p+\bar{p}\to b+c}^2 \frac{|\psi_{1S}(0)|^2}{m_p} = g_{p+\bar{p}\to b+c}^2 \frac{\alpha^3 m_p^2}{8\pi} \quad \text{(A7)}$$

Reaction $a \to b + c$	Spin-weight functions $f(k_{bc})$
$0^+ \to 0^\pm 0^\pm$	1
$0^- \to 1^- 1^-$	$2m_a^2 k_{bc}^2$
$1^- \to 0^\pm 0^\pm$	$\frac{4}{3} k_{bc}^2$
$0^\pm \to 1^- 0^\pm$	$\dfrac{4m_a^2 k_{bc}^2}{3m_b^2}$
$1^- \to 1^- 0^-$	$\frac{2}{3} m_a^2 k_{bc}^2$
$1^- \to 1^- 1^-$ (a)	$\dfrac{m_a^2(m_a^2 + 2m_b^2 + 2m_c^2)k_{bc}^2}{3m_b^2 m_c^2}$
$1^- \to 1^- 1^-$ (b)	$\dfrac{2k_{bc}^2}{3}\left(3 + \dfrac{m_a^2 k_{bc}^2}{m_b^2 m_c^2}\right)$

Table 4: The spin-weight functions $f(k_{bc})$, Eq.(A4), for two particle decays. For the three-vector-meson vertex Eq.(A3), the two cases correspond to the situations considered in Section C: (a) $g_v^{(12)} = g_v^{(1)} = -g_v^{(2)}$, $g_v^{(3)} = 0$ and (b) $g_v^{(1)} = g_v^{(2)} = 0$, $g_v^{(3)} \neq 0$, both assuming $m_b = m_c$.

Process	Ref.	Branching ratio BR	g_{abc}
$p\bar{p}(^1S_0) \to \phi\rho$	[2]	$(3.4 \pm 1.0) \cdot 10^{-4}$	$g_{a\to\phi\rho} = 8.71 \cdot 10^{-4}$
$p\bar{p}(liq.) \to \omega\rho^0_{\to\pi+\pi-}$	[26]	$(2.26 \pm 0.23) \cdot 10^{-2}$	$g_{a\to\omega\rho} = 2.77 \cdot 10^{-3}$
$p\bar{p}(S \to {}^3S_1) \to \phi\pi^0$	[7]	$(6.5 \pm 0.6) \cdot 10^{-4}$	$g_{a\to\phi\pi} = 3.43 \cdot 10^{-4}$
	[5]	$(5.5 \pm 0.7) \cdot 10^{-4}$	
	[8]	$(7.57 \pm 0.62) \cdot 10^{-4}$	
	[2]	$(4.0 \pm 0.8) \cdot 10^{-4}$	
$p\bar{p}(S \to {}^3S_1) \to \omega\pi^0$	[3]	$(5.7 \pm 0.5) \cdot 10^{-3}$	$g_{a\to\omega\pi} = 7.59 \cdot 10^{-4}$
	[27]	$(5.2 \pm 0.5) \cdot 10^{-3}$	
$p\bar{p} \to \rho\rho$	[12]	$2.4 \cdot 10^{-2}$	$g^{(1)}_{\rho\rho} = 8.21 \cdot 10^{-4}$ $g^{(2)}_{\rho\rho} = 9.79 \cdot 10^{-4}$ GeV^{-1}
$p\bar{p} \to K^*\bar{K}, \bar{K}^*K$	[28]	$0.23 \cdot 10^{-2}$	$g_{K^*\bar{K}} = 7.0 \cdot 10^{-4}$ GeV^{-1}

Table 5: The experimental branching ratios for the two-meson $p\bar{p}$ annihilation at rest and the corresponding coupling constants used in the present calculations. The coupling constants are normalized to the total width of the atomic $(p\bar{p})_{1S}$ state $\Gamma_{(p\bar{p})_{1s}} = 1$ keV (the singlet–to–triplet ratio $1:3$ is assumed for the $p\bar{p}$ spin fractions).

A.2 Vertices for three-meson annihilation

In the case of three-particle transitions $a \to x + y + z$ we consider reactions of the following types

$$\begin{aligned} 0^- &\to 0^- 0^- 0^- \\ 0^- &\to 1^- 0^- 0^- \\ 1^- &\to 1^- 0^- 0^- \end{aligned}$$

The corresponding amplitudes with a minimal number of derivatives read

$$\langle \phi_x \phi_y \phi_z | T | \phi_a \rangle = g_{pppp} \tag{A8}$$

$$\langle \phi_x \phi_y V_z | T | \phi_a \rangle = g_{pppv}\, \epsilon_{\mu\nu\alpha\beta}\, p_a^\mu p_x^\nu p_y^\alpha \varepsilon_z^\beta \tag{A9}$$

$$\langle \phi_x \phi_y V_z | T | V_a \rangle = g_{vppv}\, \varepsilon_a \cdot \varepsilon_z \tag{A10}$$

The coupling constants g_{axyz} are related to the three-body transition widths $\Gamma_{a\to xyz}$ by

$$\Gamma_{a\to xyz} = \frac{g_{axyz}^2}{2m_a(2\pi)^5} \int w\; d\Phi_3. \tag{A11}$$

where w are the kinematical factors given in Table 6 and the three-body phase space $d\Phi_3$ is defined by Eq.(3).

For the $p\bar{p}(0^-) \to \pi\pi\pi$ vertex we have two cases considered in Sect. 2. The vertex that is completely symmetric in the isospin of the $\pi\pi\pi$ system corresponds to Eq.(A8) with the coupling constant $g_{3\pi}^A$. The vertex with the mixed symmetry is given by

$$\langle \pi^+\pi^0\pi^- | T | p\bar{p}(J=0^-, I=1) \rangle = g_{3\pi}^B (p_0 \cdot p_+ + p_0 \cdot p_- - 2p_+ \cdot p_+) \tag{A12}$$

where p_+, p_0, p_- are the four-momenta of the corresponding pions.

The numerical values of the coupling constants for the three-meson $p\bar{p}$ annihilation are summarized in Tab. 7 together with the corresponding experimental branching ratios.

B Evaluation of Amplitudes with Spin

The on-shell approximation Fig. 1(b) for particles with spin leads to the following expression for the covariant amplitudes T_{UA} replacing the spinless case of Eq.(2)

$$T_{UA} = \frac{i g_a g_b g_c g_d}{2(2\pi)^5} \int \frac{w(p_x, p_y, p_z) d\Phi_3(p_a, p_x, p_y, p_z)}{(p_v^2 - m_v^2 + i\epsilon)(p_w^2 - m_w^2 + i\epsilon)} \tag{B1}$$

The evaluation of the spin–weight functions $w(p_x, p_y, p_z)$ can be done on the amplitude level using a decomposition of the spin functions into covariant tensor structures built of the external momenta p_a and p_b. The corresponding computations have been done using symbolic codes written in MAPLE and were verified by hand for several cases. As a further, independent check we have determined helicity amplitudes in an explicit polarization basis, see e.g. Ref. [32], and calculated the sum of the squared helicity amplitudes.

Reaction $a \to x+y+z$	Spin-weight factor w
$0^- \to 0^- 0^- 0^-$	1
$0^- \to 1^- 0^- 0^-$	$m_a^2(\mathbf{k}_x^2\mathbf{k}_y^2 - (\mathbf{k}_x\mathbf{k}_y)^2)$
$1^- \to 1^- 0^- 0^-$	$1 + \frac{1}{3}\frac{k_x^2}{m_x^2}$

Table 6: Spin–weight functions w for different three-body final states. The $\mathbf{k}_x$ and $\mathbf{k}_y$ are the 3-momenta of particles x and y in the CMS. The interaction terms are defined in Eqs.(A8-A10).

Process	Ref.	Branching ratio BR	$\lvert g_{abcd}\rvert$
$p\bar{p}(liq.) \to \omega\pi\pi$	[26]	0.066 ± 0.006	
$p\bar{p}(S \to {}^1S_0) \to \omega\rho^0_{\to\pi^+\pi^-}$	[26]	0.0226 ± 0.0023	$g_{p\bar{p}({}^1S_0)\to\omega\pi\pi} = 0.21$ GeV^{-3}
$p\bar{p}(S) \to \pi^0\pi^+\pi^-$	[29]	0.066 ± 0.008	
$p\bar{p}(S \to {}^1S_0) \to (\pi^0\pi^+\pi^-)_{\mathrm{p}h.sp.}$		$0.066 \cdot (0.083 \pm 0.029)$	$g^A_{p\bar{p}({}^1S_0)\to 3\pi} = 0.015$
$p\bar{p}(S \to {}^1S_0) \to \rho^\pm\pi^\mp$		$0.066 \cdot (0.014 \pm 0.006)$	$g^B_{p\bar{p}({}^1S_0)\to(3\pi)} = 0.0056$
$p\bar{p}(liq.) \to \pi^0\pi^+\pi^-$	[30]	0.069 ± 0.004	
$p\bar{p}(liq.) \to \pi^0\pi^0\pi^0$	[6]	$(6.2 \pm 1.0) \cdot 10^{-3}$	
$p\bar{p}(S \to {}^1S_0) \to \pi^0\pi^0\pi^0$		$6.2 \cdot 10^{-3} \cdot 0.54$	$g^A_{p\bar{p}({}^1S_0)\to 3\pi} = 0.010$
$p\bar{p}(S \to {}^3S_1) \to \rho_{\to\pi^+\pi^-}\sigma_{\to\pi^+\pi^-}$	[31]	$7.61 \cdot 10^{-2} \cdot 0.50$	$g_{p\bar{p}({}^3S_1)\to\rho\pi\pi} = 0.043$

Table 7: The experimental branching ratios for the three–meson $p\bar{p}$ annihilation at rest and the corresponding coupling constants used in the present calculations. The coupling constants are normalized to the total width of the atomic $(p\bar{p})_{1S}$ state $\Gamma_{(p\bar{p})_{1s}} = 1$ keV and the singlet–to–triplet ratio $1:3$ is assumed for the $p\bar{p}$ spin fractions.

B.1 Invariant Amplitudes and General Tensor Decomposition

The covariant integrals over internal momenta p_x^μ and p_y^μ can generally be expressed in terms of linearly independent tensors constructed of the external momenta, p_a^μ and p_b^μ multiplied by invariant amplitudes. For the one-loop diagrams (see Tables 1 and 2) we introduce the following notation

$$\langle p_x^\mu \rangle = \int f(p_x, p_a, p_b)\, p_x^\mu \, d^4 p_x \tag{B2}$$

where the scalar function $f(p_x, p_a, p_b)$ is defined by a direct calculation of the one loop diagram. The general form of this integral is given by

$$\langle p_x^\mu \rangle = I_1^{(1)}\, p_a^\mu + I_2^{(1)}\, p_b^\mu \tag{B3}$$

where the coefficients $I_1^{(1)}$ and $I_2^{(1)}$ can be found straightforwardly:

$$I_1^{(1)} = \langle \frac{k_b E_x - E_b k_x z_x}{m_a k_b} \rangle \tag{B4}$$

$$I_2^{(1)} = \langle \frac{k_x z_x}{k_b} \rangle \quad . \tag{B5}$$

Here the notation $\langle \ldots \rangle$ is defined similarly to Eq.(B2) with the same scalar function $f(p_x, p_a, p_b)$. The second order expressions in the one–loop case contain in addition two products of p_a^μ and p_b^μ and the metric tensor $g^{\mu\nu}$:

$$\langle p_x^\mu p_x^\nu \rangle = I_1^{(2)}\, g^{\mu\nu} + I_2^{(2)}\, p_a^\mu p_a^\nu + I_3^{(2)} (p_a^\mu p_b^\nu + p_b^\mu p_a^\nu) + I_4^{(2)}\, p_b^\mu p_b^\nu \tag{B6}$$

where

$$I_1^{(2)} = \langle -\frac{(1 - z_x^2) k_x^2}{2} \rangle \tag{B7}$$

$$I_2^{(2)} = \langle \frac{2\,(k_x^2 z_x^2 + E_x^2) k_b^2 - 4\, E_b k_b E_x k_x z_x - (1 - 3\, z_x^2) m_b^2 k_x^2}{2\, m_a^2 k_b^2} \rangle \tag{B8}$$

$$I_3^{(2)} = \langle \frac{((1 - 3\, z_x^2) E_b k_x + 2\, k_b E_x z_x) k_x}{2\, m_a k_b^2} \rangle \tag{B9}$$

$$I_4^{(2)} = \langle -\frac{(1 - 3\, z_x^2) k_x^2}{2\, k_b^2} \rangle . \tag{B10}$$

In the case of two-loop amplitudes we have more internal degrees of freedom, and Eq.(B6) is replaced by

$$\langle p_x^\mu p_y^\nu \rangle = \int f(p_x, p_y, p_a, p_b)\, p_x^\mu\, p_y^\nu \, d^4 p_x \, d^4 p_y . \tag{B11}$$

The tensor decomposition for this expression takes the following form

$$\langle p_x^\mu p_y^\nu \rangle = I_1^{(xy)}\, g^{\mu\nu} + I_2^{(xy)}\, p_a^\mu p_a^\nu + I_3^{(xy)} (p_a^\mu p_b^\nu + p_b^\mu p_a^\nu) + I_4^{(xy)}\, p_b^\mu p_b^\nu . \tag{B12}$$

where

$$I_1^{(xy)} = \langle -\frac{(Z - z_x z_y) k_x k_y}{2} \rangle \tag{B13}$$

$$I_2^{(xy)} = \langle \frac{2\,(k_x k_y z_x z_y + E_x E_y) k_b^2 - 4\,E_b k_b E_x k_x z_x - (Z - 3\,z_x z_y) m_b^2 k_x k_y}{2\,m_a^2 k_b^2} \rangle \tag{B14}$$

$$I_3^{(xy)} = \langle \frac{((Z - 3\,z_x z_y) E_b k_x + 2\,k_b E_x z_y) k_y}{2\,m_a k_b^2} \rangle \tag{B15}$$

$$I_4^{(xy)} = \langle -\frac{(Z - 3\,z_x z_y) k_x k_y}{2\,k_b^2} \rangle . \tag{B16}$$

A generalisation to tensors of higher rank is straightforward. In particular, the following expressions for a rank three tensor appear in the two–loop diagrams:

$$I_7^{(yxx)} = \langle \frac{(z_x Z - z_y) k_x^2 k_y}{2} - \frac{((Z - z_x z_y) E_x k_x k_y - (1 - z_x^2) E_y k_x^2) k_b}{2 E_b} \rangle \tag{B17}$$

$$I_7^{(yxy)} = \langle \frac{(z_x - z_y Z) k_x k_y^2}{2} + \frac{((Z - z_x z_y) E_x k_x k_y - (1 - z_y^2) E_x k_y^2) k_b}{2 E_b} \rangle \tag{B18}$$

The different topologies of the two-loop diagrams involving vector and pseudoscalar mesons are shown in Fig.2. The corresponding complete spin weight functions Eq.(B1) for the diagrams A–D are listed below.

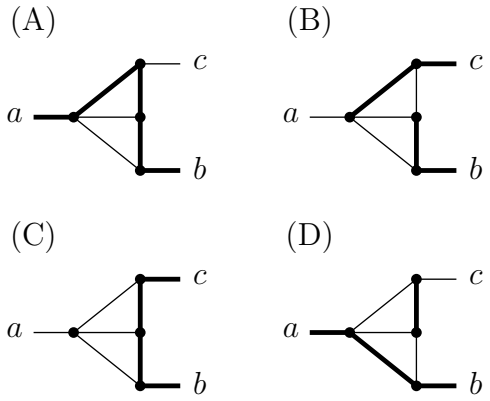

Figure 2: Different three-meson doorway processes involving pseudoscalar particles (thin lines) and vector particles (thick lines).

$$w_A(k_x, k_y, z_x, z_y) = (k_b E_y + E_c k_y z_y)(k_b E_x - E_b k_x z_x) + \tag{B19}$$
$$+ \quad \frac{1}{2 m_a k_b} \Big\{ - \Big[((z_x + z_y Z) E_c k_y + (z_x z_y + Z) k_b E_y)\, E_b^2 + (z_x z_y + Z) E_c^2 k_b E_x \Big]\, k_x k_y +$$
$$+ \quad \Big[\Big((z_x + z_y Z) k_y^2 + 2 m_y^2 z_x \Big)\, E_x k_x - \Big((z_y + z_x Z) k_x^2 + 2 m_x^2 z_y \Big)\, E_y k_y \Big]\, k_b^2 -$$

$$
\begin{aligned}
- \quad & \Big[\Big((z_y^2+1)k_y^2+2m_y^2+(z_xz_y-Z)k_xk_y\Big)E_x + \\
& +\Big((z_x^2+1)k_x^2+2m_x^2+(z_xz_y-Z)k_xk_y\Big)E_y\Big]k_b^3 + \\
+ \quad & \Big[(z_y+z_xZ)E_c^2k_x^2k_y+\Big((z_x+z_yZ)E_xk_xk_y^2-(z_y+z_xZ)E_yk_x^2k_y+ \\
& +\Big((2k_xz_xk_yz_y+(z_y^2+1)k_y^2)E_x+(2k_xz_xk_yz_y+(z_x^2+1)k_x^2)E_y\Big)k_b\Big)E_c + \\
& +\Big(2(k_xz_x+k_yz_y)E_xE_y+((z_y^2+1)k_y^2+2m_y^2+(z_xz_y-Z)k_yk_x)k_xz_x\Big)k_b^2 + \\
& +\Big((z_xz_y+Z)E_xE_yk_xk_y+((z_xz_yZ-z_x^2-z_y^2-Z^2)k_y^2-(z_x^2+1)m_y^2)k_x^2\Big)k_b\Big]E_b - \\
- \quad & \Big[\Big(2(k_xz_x+k_yz_y)E_xE_y+((z_x^2+1)k_x^2+2m_x^2+(z_xz_y-Z)k_xk_y)k_yz_y\Big)k_b^2- \\
& -\Big((z_xz_y+Z)E_xE_yk_xk_y+((z_xz_yZ-z_x^2-z_y^2-Z^2)k_x^2-(z_y^2+1)m_x^2)k_y^2\Big)k_b\Big]E_c\Big\}.
\end{aligned}
$$

$$
\begin{aligned}
w_B(k_x,k_y,z_x,z_y) &= -2\left(I_1^{(2)}+I_7^{(yxx)}\frac{E_b}{m_ak_b}\right)\left(p_a\cdot p_y\; p_c\cdot p_y-p_a\cdot p_c\; m_y^2\right)+ \\
&\quad +2\left(I_1^{(xy)}+I_7^{(yxy)}\frac{E_b}{m_ak_b}\right)(p_a\cdot p_y\; p_c\cdot p_x-p_a\cdot p_c\; p_x\cdot p_y) \qquad \text{(B20)} \\
w_C(k_x,k_y,z_x,z_y) &= I_1^{(1)}(p_c\cdot p_w\; p_y\cdot p_v-p_c\cdot p_v\; p_y\cdot p_w)+I_1^{(2)}p_y\cdot p_w-I_1^{(xy)}p_y\cdot p_v+ \\
&\quad +\left(I_7^{(yxx)}p_c\cdot p_w-I_7^{(yxy)}p_c\cdot p_v\right)\frac{E_b}{m_ak_b} \qquad \text{(B21)} \\
w_D(k_x,k_y,z_x,z_y) &= I_1^{(1)}\left[\frac{(m_y^2-m_c^2)(m_y^2-m_c^2+2(p_a-p_x)\cdot(p_c-p_y)}{m_w^2}-\right. \\
&\quad \left.-(p_c+p_y)^2+2(p_a-p_x)\cdot(p_c+p_y))\right] \qquad \text{(B22)}
\end{aligned}
$$

The isospin factors resulting from the summation over all intermediate states in the diagrams of Tables 1 and 2 are listed in Table 8.

Mechanism	Isospin factor
$p\bar{p}(^3S_1)\to\pi\rho\pi\to\phi\pi^0$	1
$p\bar{p}(^3S_1)\to\rho\pi\pi\to\phi\pi^0$	$\frac{1}{3}$
$p\bar{p}(^1S_0)\to\pi\pi\pi\to\phi\rho^0$ (A)	$\frac{5}{\sqrt{3}}$
$p\bar{p}(^1S_0)\to\pi\pi\pi\to\phi\rho^0$ (B)	$\sqrt{3}$
$p\bar{p}(^1S_0)\to\pi\pi\omega\to\phi\rho^0$	$\sqrt{\frac{2}{3}}$
$p\bar{p}(^1S_0)\to\pi\omega\pi\to\phi\rho^0$	$-\sqrt{\frac{2}{3}}$

Table 8: The isospin factors corresponding to the three-meson door–way mechanisms $p\bar{p}\to xyz\to\phi X$.

C Re-evaluation of $p\bar{p} \to \rho\rho \to \phi\pi$

For the $\rho\rho$ diagram the effective Langrangian is not unique since the annihilation vertex $p\bar{p} \to \rho\rho$ allows for two invariant couplings with minimal number of derivatives. As in [13], these are denoted by

$$T^{(1)}_{p\bar{p}\to\rho\rho} = g_1 \left(\varepsilon_{p\bar{p}}\cdot\varepsilon_x \, k_{p\bar{p}}\cdot\varepsilon_y - \varepsilon_{p\bar{p}}\cdot\varepsilon_y \, k_{p\bar{p}}\cdot\varepsilon_x\right) \quad \text{(C1)}$$

$$T^{(2)}_{p\bar{p}\to\rho\rho} = g_2 \, \varepsilon_{p\bar{p}}\cdot k_x \, \varepsilon_x\cdot\varepsilon_y \quad \text{(C2)}$$

where k_x and k_y are the four-momenta of particles x and y and $\varepsilon_{p\bar{p}}$, ε_x and ε_y are the polarization vectors of the corresponding particles. In [13] the two cases were calculated separately. Here we consider the coherent sum of both amplitudes

$$T_{p\bar{p}\to\rho\rho} = T^{(1)}_{p\bar{p}\to\rho\rho}\cos\theta + T^{(2)}_{p\bar{p}\to\rho\rho}\sin\theta \quad \text{(C3)}$$

where the total strength is normalized to $BR(p\bar{p} \to \rho\rho) = 2.4$ % from the theoretical estimate in [12]. Figure 3 shows the result of the calculations of the branching ratio for the $\phi\pi^0$ final state (including finite width effects) for the full space of parameters g_1, g_2. To check the self consistency of the door–way calculations the contribution of the $\rho\rho$ intermediate state to the $\omega\pi^0$ production has been evaluated as well. Since the $\omega\pi^0$ channel is not suppressed on the tree-level, it is gratifying that the one–loop corrections turn out to be small in comparison with the experimental data for this channel. At the same time, the contribution to the OZI suppressed channel $\phi\pi^0$ is very significant for a broad range of the relative strength of g_1 and g_2.

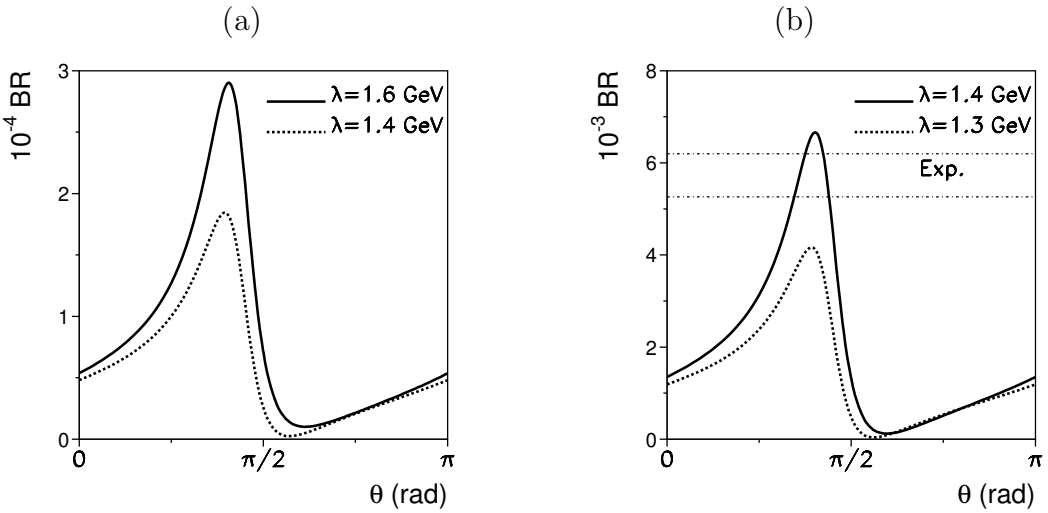

Figure 3: The branching ratios corresponding to the door–way $\rho\rho$ mechanism for (a) $\phi\pi^0$ and (b) $\omega\pi^0$ production from $p\bar{p}(^3S_1)$ annihilation. The parameter ϑ defines the relative strength of the two couplings in the $p\bar{p} \to \rho\rho$ vertex, see Eqs. C1 and C2.

References

[1] C. Amsler and F. Myhrer, Ann. Rev. Nucl. Part. Sci. **44**, 219 (1991)

[2] ASTERIX, J. Reifenröther et al., Phys. Lett. **B 267**, 299 (1991)

[3] C. Amsler et al., Phys. Lett. **B 311**, 371 (1993)

[4] Crystal Barrel, C. Amsler et al., Z. Phys. **C 58**, 175 (1993); K. Braune, Nucl. Phys. **A 558**, 269c (1993)

[5] Crystal Barrel, C. Amsler et al., Phys. Lett. **B 346**, 363 (1995)

[6] Crystal Barrel, C. Amsler et al., Phys. Lett. **B 342**, 433 (1995)

[7] C. Amsler, Rev. Mod. Phys. **70**, 1293 (1998)

[8] V. Alberico et al., Phys.Lett. **B 438**, 430 (1998)

[9] J. Ellis, E. Gabathuler and M. Karliner, Phys. Lett. **B 217**, 173 (1989)

[10] J. Ellis and M. Karliner, Phys. Lett. **B 313**, 131 (1993); **B 341**, 397 (1995)

[11] J. Ellis, M. Karliner, D.E. Kharzeev and M.G. Sapozhnikov, Phys. Lett. **B 353**, 319 (1995)

[12] A. Cieply, M.P. Locher and B.S. Zou, Z. Phys. **A 345**, 41 (1993)

[13] Yang Lu, B.S. Zou and M.P. Locher, Z. Phys. **A 345**, 207 (1993)

[14] M.P. Locher, Yang Lu and B.S. Zou, Z. Phys. **A 347**, 281 (1994)

[15] D. Buzatu and F.M. Lev, Phys. Lett. **B 329**, 143 (1994)

[16] D. Buzatu and F.M. Lev, Phys. Rev. **C 51**, R2893 (1995)

[17] D. Buzatu and F.M. Lev, Phys. At. Nucl. **58**, 480 (1995)

[18] M.P. Locher and Yang Lu, Z. Phys. **A 351**, 83 (1995)

[19] O. Gortchakov, M.P. Locher, V.E. Markushin and S. von Rotz, Z. Phys. **A 353**, 447 (1996)

[20] V.E. Markushin and M.P. Locher, Eur. Phys. J. **A 1**, 91 (1998)

[21] V.E. Markushin, Nucl. Phys. B (Proc. Suppl.) **56A**, 303 (1997); Nucl. Phys. **A655**, 185 (1999)

[22] S. von Rotz, Ph. D. Thesis, University of Zürich (1998).

[23] A. Pais, Ann. of Phys. **9**, 548 (1960)

[24] Review of particle properties, Eur. Phys. J. **C 3**, 110 (1998)

[25] H.J. Lipkin, Nucl. Phys. **B 244**, 147 (1984)

[26] R. Bizzarri et al., Nucl. Phys. **B 14**, 169 (1969)

[27] M. Chiba et al., Phys Lett. **B 202**, 447 (1988)

[28] B. Conforto et al., Nucl Phys. **B3**, 469 (1967)

[29] B. May et al., Z. Phys. **C 46**, I 191 (1990); Z. Phys. **C 46**, II 203 (1990)

[30] M. Forster. et al., Nucl. Phys. **B6**, 107 (1968)

[31] A. Bertin et al., Phys. Lett. **B 414**, 220 (1997)

[32] W. Grein, A. König, P. Kroll, M.P. Locher and A. Svarc, Ann. Phys. **153**, 301 (1984)